Enhanced Charge Collection for Splitting of Water Enabled by an Engineered Three-Dimensional Nanospike Array

ARTICLE *in* THE JOURNAL OF PHYSICAL CHEMISTRY C · SEPTEMBER 2014

Impact Factor: 4.77 · DOI: 10.1021/jp507800t

THE JOURNAL OF PHYSICAL CHEMISTRY C

Article

pubs.acs.org/JPCC

Enhanced Charge Collection for Splitting of Water Enabled by an Engineered Three-Dimensional Nanospike Array

Yongcai Qiu,[†,‡,§,∥] Siu-Fung Leung,[†,∥] Zhanhua Wei,[†] Qingfeng Lin,[‡] Xiaoli Zheng,[†] Yuegang Zhang,[§] Zhiyong Fan,*[,‡] and Shihe Yang*[,†]

[†]Department of Chemistry, and [‡]Department of Electronic and Computer Engineering, The Hong Kong University of Science and Technology, Clear Water Bay, Kowloon, Hong Kong, People's Republic of China

[§]*i*-Lab, Suzhou Institute of Nano-Tech and Nano-Bionics, Chinese Academy of Sciences, Suzhou, Jiangsu 215123, China

Supporting Information

ABSTRACT: Photoelectrochemical (PEC) water splitting is a promising method of converting solar energy to hydrogen fuel from water using photocatalysts. Despite much effort in preparing mesoporous thin films on planar substrates, relatively little attention has been paid to their deposition on three-dimensional (3D) substrates, which could improve electron collection and enhance light-trapping. Here, we report the first synthesis of hierarchically branched anatase TiO_2 nanotetrapods, achieved by dissolution and nucleation processes on a ZnO nanotetrapods template. When used as a photoanode for efficient PEC water splitting, the unique branched anatase TiO_2 nanotetrapods yielded a photocurrent density of 0.54 mA cm^{-2} at applied potential of 0.35 V vs RHE, much higher than that of commercial TiO_2 nanoparticles under otherwise identical conditions. Moreover, when the nanotetrapods were deposited on an ordered, purposely engineered 3D F-doped tin oxide (FTO) nanospike array, the photocurrent density was upgraded to 0.72 mA cm^{-2}. This large photocurrent enhancement can be attributed to the ultrahigh contact surface area with the electrolyte, which is bequeathed by the hierarchically branched TiO_2 nanotetrapods with a skin layer of vertically aligned ultrathin nanospines, as well as the short charge transport distance and enhanced light-trapping due to the peculiar 3D FTO nanospike array we have engineered by design.

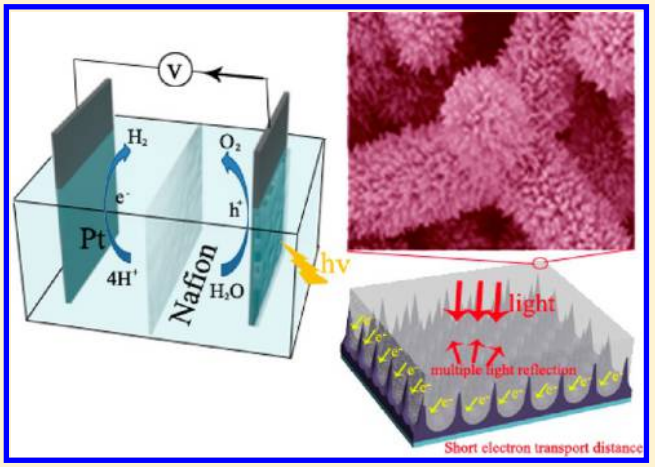

1. INTRODUCTION

In the past decades, considerable interest in photoelectrochemical (PEC) water splitting[1−13] has mounted due to the global environmental problems and energy issues. PEC water splitting is a promising method of utilizing solar energy to convert water into hydrogen fuel using photocatalysts. Metal oxides,[14−27] such as WO_3,[15] TiO_2,[16−21] and Fe_2O_3,[19,22] are conspicuous candidates for PEC water splitting due to their high resistance to photocorrosion, potential for high efficiency, durability, and low cost. Substantial efforts have been invested in promoting their PEC performance based on nanoparticle (NP) films due to their large surface area to volume ratios. However, such NP-based films often suffer from serious charge recombination due to severe carrier trapping at numerous grain boundaries. To address this issue, researchers have sought to use one-dimensional (1D) metal oxide arrays grown on conductive substrates in view of their fast vectorial electron transport, facile charge separation, and high photon-capturing capability.

Recently, TiO_2 nanotubes,[17,18] nanowires,[20,21] and their branched varieties[23] have been successfully prepared to improve the PEC water splitting performance. Indeed, the electronic loss was found to be much smaller than that of NPs as charges can more quickly reach the conductive electrodes before recombination. However, the relatively low surface areas of those 1D materials largely limit their performance. To further improve the PEC performance, we herein propose a newly developed photoanode architecture by depositing hierarchically branched TiO_2 nanotetrapods (NTs) on an engineered three-dimensional (3D) F-doped tin oxide (FTO) nanospike array. This architecture is based on two key materials innovations. One is the synthesis of the hierarchically branched TiO_2 NTs, and the other is the fabrication of the purpose-built 3D FTO nanospike array. It also embodies a number of design considerations for a PEC water splitting photoanode: (i) the constructed TiO_2 tetrapods network is mechanically robust and enables excellent electron transport; (ii) the TiO_2 branches enhance solar light absorption due to the improved light scattering; (iii) the photoactive materials deposited on 3D conductive nanospike array have fast charge separation[28,29] due to short charge transport distance; and (iv) the substrate

Received: August 4, 2014
Revised: September 10, 2014
Published: September 10, 2014

   dx.doi.org/10.1021/jp507800t | *J. Phys. Chem. C* 2014, 118, 22465−22472

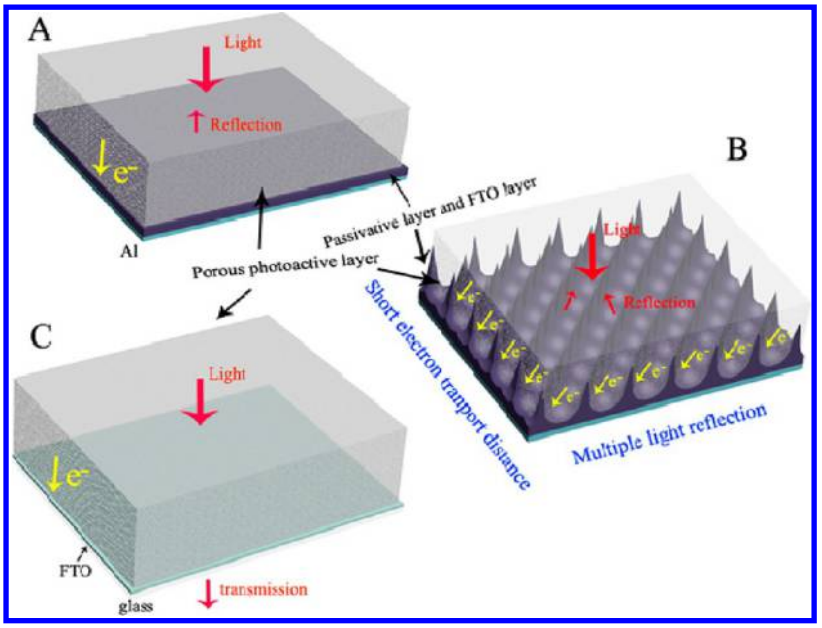

Figure 1. Schematic illustration of light and electron transport routes in three different substrates highlighting the advantages of the 3D nanospike array in terms of electron transport and light trapping. (A) Porous photoactive layer deposited on Al-based flat substrate. (B) Porous photoactive layer deposited on Al-based spiked substrate. (C) Porous photoactive layer deposited on FTO-coated glass substrate. The advantages of our FTO-coated spiked photoelectrode (B) are characterized by enhanced multiple light-reflection and short electron transport distance as compared to the planar FTO-coated flat Al photoelectrode (A) and FTO-coated flat glass photoelectrode (C).

comprising periodic 3D nanospikes[30−33] has excellent light trapping capability (see Figure 1).

Most recently, we reported a photoelectrode arising from the secondary branched N-doped ZnO NTs,[34] which reached a maximum photoelectrode conversion efficiency of 0.31%. However, the relatively low stability due to photocorrosion is an intrinsic limitation of ZnO materials. On the contrary, TiO_2 is much more stable in aqueous solution under irradiation, which was first demonstrated with a semiconductor−liquid junction (SCLJ)[1] as a photoelectrode in 1972. Therefore, converting the ZnO nanotetrapods (NTs) network to that of TiO_2 network is a potentially viable strategy for fabricating PEC photoelectrodes,[35] which not only preserves the expedient network structure of the ZnO template but also conferred the excellent photocorrosion stability. Here, the TiO_2 NTs can be deposited on ordered 3D FTO-coated spiked substrates as photoelectrodes for PEC water splitting.

2. EXPERIMENTAL SECTION

Materials. Aluminum foil (0.25 mm thick, 99.99% purity) was obtained from Alfa Aesar. Epoxy glue (Norland Optical Adhesive 81) was purchased from Norland Products Inc. Silicone elastomer and the curing agent were purchased from Dow Corning. All other chemicals are products of Sigma-Aldrich.

Nanospike Fabrication. Aluminum (Al) foil was cut into 1 cm × 2 cm pieces and cleaned in acetone and isopropyl alcohol. The sheets were electrochemically polished in a 1:3 (v:v) mixture of perchloric acid and ethanol for 2 min at 10 °C. The polished Al sheets were imprinted by silicon mold (squarely ordered pillar array with height of 200 nm and with a pitch of 1.5 μm) with a pressure of ∼2 × 10^4 N cm^{-2} to initiate the perfectly ordered AAM growth. The Al sheets then were placed in a home-built anodization setup. Anodization was carried out at a 600 V voltage and in a mixture of 1:1 v/v% of the 2 wt % citric acid and ethylene glycol. Carbon rod was used as the counter-electrode. For the exposure of 3D Al NSP arrays, the AAM film was etched in a mixture of chromiumacid (1.5 wt %) and phosphoric acid (6 wt %) solutions at 100 °C for 1 h. After etching, the 3-D Al NSP array chips were cleaned with DI water and blown dry with air for the subsequent thin film deposition.

Synthesis of ZnO Nanotetrapods. The ZnO nanotetrapod powder was synthesized by the metal vapor transport-oxidation method we reported previously,[37] except for small modifications for high loading of Zn source and thus high yield of the ZnO nanotetrapod product. For ZnO nanotetrapods film preparation, 1 g of ZnO nanotetrapods powder was first dissolved in 10 mL of 1-butanol to form a sufficiently viscous paste. The doctor blade technique then was employed to spread this paste onto a conductive glass substrate (FTO-coated glass, 14 Ω $\square^{-1}$).

Synthesis of TiO_2 Nanotetrapods. The ZnO NTs substrate was immersed in an aqueous solution of $(NH_4)_2TiF_6$ and H_3BO_3 (1:3) at different reaction times, and then rinsed with ethanol and dried in air.

Characterizations. Morphologies of the nanomaterials were directly examined by SEM using a JEOL6700F at an accelerating voltage of 5 kV. TEM observations were carried out on a JEOL 2010F microscope operating at 200 kV. Diffused reflectance spectra were carried out on the same film samples using a PerkinElmer UV/vis spectrophotometer (model Lambda 20). The film thickness was determined by a Tencor Alpha-Step 200 surface profiler system. The light source (Oriel solar simulator, 450 W Xe lamp, AM 1.5 global filter) was calibrated to 1 sun (100 mW cm^{-2}) using an optical power meter (Newport, model 1916-C) equipped with a Newport 818P thermopile detector. The electrochemical spectra were measured by the Zahner Zennium C-IMPS system.

3. RESULTS AND DISCUSSION

The preparation of the ordered 3D FTO-coated spiked substrates is a key step for the improvement of PEC water

dx.doi.org/10.1021/jp507800t | J. Phys. Chem. C 2014, 118, 22465−22472

splitting performance. In our previous work, we have demonstrated 3D Al nanospikes (NSP),[11,30−33,36] which served as light trapping substrates for high performance and cost-effective thin film photovoltaics. It is worth pointing out that the highly ordered Al nanospikes were obtained by nanoimprint assisted anodization process (see Experimental Section and Figure S1 in the Supporting Information). Here, the ordered 3D Al spiked substrates with a pitch of 1.5 μm are selected (Figure 2A). To achieve a high PEC performance, 1 M of

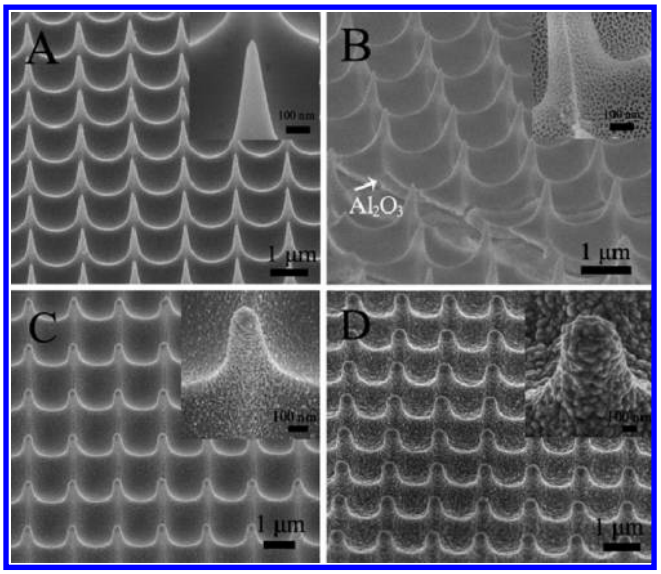

Figure 2. Scanning electron microscopic images of FTO-coated Al-based spiked nanostructures. (A) Low-magnification and (inset) high-resolution SEM images show the grown Al NSP array after etching of Al_2O_3. (B) Low-magnification and (inset) high-resolution SEM images show the formation of a passivation layer of Al_2O_3 after anodization process. (C) Low-magnification and (inset) high-resolution SEM images show a conductive layer Ti/Pt coated on the surface of Al−Al_2O_3 NSP array. (D) Low-magnification and (inset) high-resolution SEM images show a conductive and protecting layer of FTO coated on the surface of Al−Al_2O_3−Ti/Pt NSP array.

NaOH aqueous solution (pH = 13.6) was used as the electrolyte for TiO_2 PEC water splitting, and this could etch the Al metal substrate. To address this issue, we adopted several coating steps to prepare passivation layers. The passivation layers contain ∼100 nm thick porous Al_2O_3 layer, ∼150 nm thick Ti/Pt (100 + 50) metal layer, and 100 nm thick FTO layer. The porous Al_2O_3 layer was first grown by anodization process (20 V in 1.7 wt % H_2SO_4 for 10 min) (Figure 2B), and subsequently a layer of 100 nm thick Ti and 50 nm Pt was coated by magnetron sputtering (Figure 2C). Approximately 100 nm thick F-doped SnO_2 then was deposited on the spiked substrates by ultrasonic spray pyrolysis (USP) using an ethanol solution of $SnCl_4$ (0.2 M) and NH_4F (0.04 M). The uniformity of the FTO layer on the spiked substrate is evidenced in Figure 2D, suggesting that the USP technique is perfectly suitable for the FTO deposition on 3D nanostructured substrates. An optical image of the flat and spiked substrates is also shown in Supporting Information Figure S2, clearly suggesting the significantly enhanced light trapping by the spiked substrate, as validated by light-scattering spectra in Supporting Information Figure S2.

The additional branching of the TiO_2 NTs was achieved by dissolution and nucleation processes on a ZnO nanotetrapods template, as schemed in Supporting Information Figure S3. ZnO NTs[37] were prepared on the basis of our previous work. To improve the performance of PEC cells, prior to the main materials coating, a thin ∼50 nm thick interfacial TiO_2 blocking layer was deposited onto the spiked substrates by ultrasonic spray pyrolysis (USP) using an ethanol solution of titanium diisopropoxide bisacetylacetonate (TIACA) (v/v = 1/10). Afterward, the ZnO NTs were then deposited on the TiO_2-coated spiked substrate by spin coating (see Supporting Information Figure 3A and inset). The films were prepared with a thickness of ∼5 μm. The films were then immersed in a solution of $(NH_4)_2TiF_6$ and H_3BO_3 (1:3). Figure 3B shows the

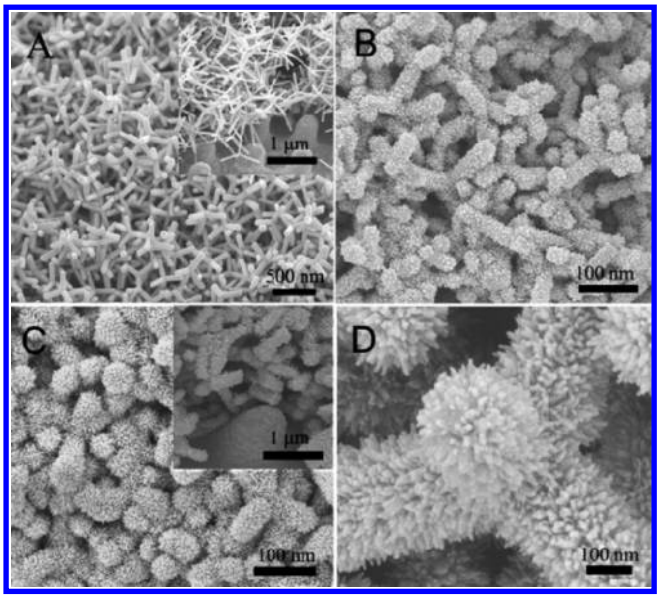

Figure 3. Microscopy of the branched TiO_2 nanotetrapods. (A) SEM images of the ZnO NTs film (inset of (A) shows its titled SEM view), (B) SEM image shows the TiO_2 NTs film obtained from immersion of ZnO NTs in a solution of $(NH_4)_2TiF_6$ and H_3BO_3 (1:3) for 20 h, and (C) SEM images show the branched TiO_2 NTs film obtained from immersion of (B) film in a fresh solution of $(NH_4)_2TiF_6$ and H_3BO_3 (1:3) for another 30 h. Inset of (C) shows its titled SEM view. (D) SEM image shows a typical branched TiO_2 NTs with numerous spines.

film morphology after immersion in the solution of $(NH_4)_2TiF_6$ and H_3BO_3 for 20 h. Clearly, the original tetrapod structure was almost retained, but the surfaces became rough with numerous spines and the arm diameter became thicker in sharp contrast to those of the templating ZnO NTs (Figure 3A). After reimmersion into a fresh solution of $(NH_4)_2TiF_6$ and H_3BO_3 for another 30 h, longer spines and much thicker NTs were obtained, which resulted in almost a full filling of the remaining cavities, as observed in Figure 3C. A typical SEM image of the sample (Figure 3D) shows that the secondary branches were grown on the NTs with lengths ranging from 100 to 300 nm. The grown structures were subjected to powder XRD investigation. It can be concluded that the ZnO NTs were transformed into anatase TiO_2 (JCPDS card no. 21-1272)[38] after thermal treatment of the branched NTs at 500 °C for 1 h, as shown in Supporting Information Figure 3A.

To investigate the growth mechanism of the branched anatase TiO_2 NTs, we carried out the time-dependent experiments based on TEM and EDS analyses (Supporting Information Figure S5). Shown in Figure 4 are TEM images, which track the course of dissolution of ZnO and nucleation of

dx.doi.org/10.1021/jp507800t | J. Phys. Chem. C 2014, 118, 22465−22472

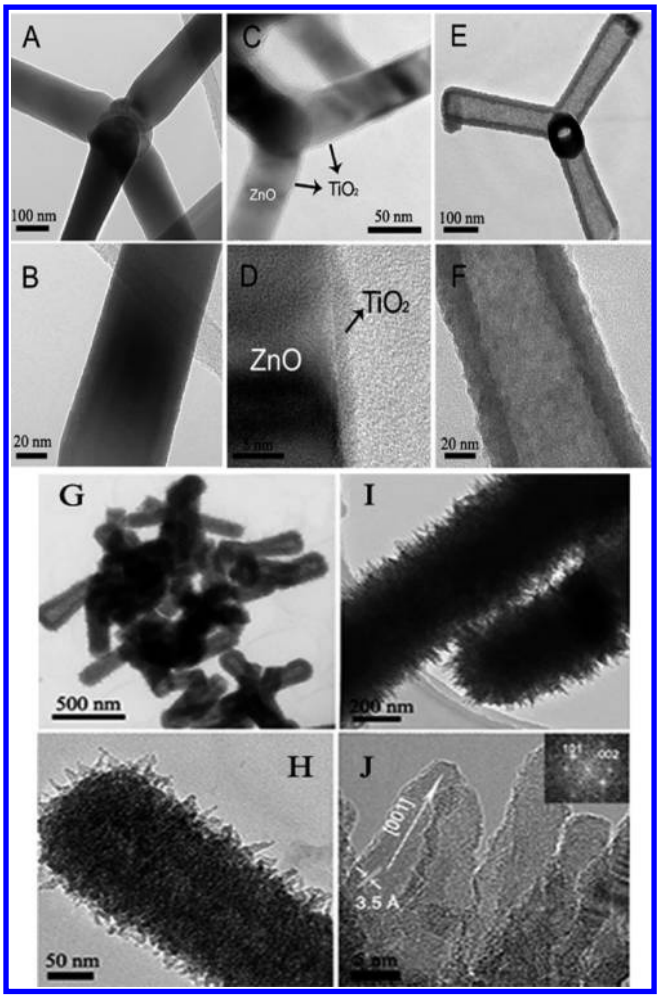

Figure 4. Electron microscopic images tracking the course of dissolution of ZnO and nucleation of TiO_2. (A) Low- and (B) high-magnification TEM images show the pristine ZnO NTs. (C) Low- and (D) high-magnification TEM images show the ZnO NTs immersed in a solution of $(NH_4)_2TiF_6$ and H_3BO_3 (1:3) for 2 min. (E) Low- and (F) high-magnification TEM images show the hollow TiO_2 NTs obtained from immersion of ZnO NTs in the solution of $(NH_4)_2TiF_6$ and H_3BO_3 (1:3) for 60 min. (G) Low- and (H) high-magnification TEM images show the TiO_2 NTs with short nanorods obtained from immersion of ZnO NTs in the solution of $(NH_4)_2TiF_6$ and H_3BO_3 (1:3) for 20 h. (I) Low- and (D) high-magnification TEM images show the TiO_2 NTs with long nanorods obtained from immersion of the sample (G) in a fresh solution of $(NH_4)_2TiF_6$ and H_3BO_3 (1:3) for another 30 h. The inset of (J) is a SAED pattern taken from the corresponding nanorod.

TiO_2. After being immersed in the solution of $(NH_4)_2TiF_6$ and H_3BO_3 (1:3) for 2 min, the ZnO NT surfaces were covered with a thin layer of TiO_2 ~1 nm thick (Figure 3C and D) in sharp contrast to those of the pristine ZnO NTs (Figure 4A and B). EDS analysis shown in Supporting Information Figure S5B has revealed the appearance of new Ti peaks as compared to the pristine ZnO NTs (Supporting Information Figure S5A). On prolonging the reaction time for 60 min, hollow TiO_2 NTs have formed due to the dissolution of ZnO NTs and the peripheral nucleation of TiO_2 (Figure 4E and F). EDS analysis shown in Supporting Information Figure S4C shows that the Ti peaks are dominant, indicating that almost all ZnO has been dissolved. Possible reaction processes[39] are shown below:

$$TiF_6^{2-} + 2H_2O \rightleftharpoons TiO_2 + 4H^+ + 6F^- \quad (1)$$

$$BO_3^{3-} + 6H^+ + 4F^- \rightleftharpoons 3H_2O + BF_4^- \quad (2)$$

$$ZnO + 2H^+ \rightarrow Zn^{2+} + H_2O \quad (3)$$

When the solution of $(NH_4)_2TiF_6$ and H_3BO_3 comes into contact with the ZnO surfaces, H^+ ions are consumed by ZnO, resulting in the formation of TiO_2 on the surfaces of ZnO (Figure 4C and D) according to reactions 1 and 3. Meanwhile, the hazardous F^- ions react with BO_3^{3-} ions in the acidic condition, leading to the formation of BF^{4-}, as expressed in eq 2.

Interestingly, on prolonging the reaction time to 20 h, more TiO_2 grew not only inside but also outside the TiO_2 NT tubes, resulting in the growth of TiO_2 NTs with a thicker diameter (Figure 4G). Also, spines sprouted from the surfaces, and the lengths ranged from 10 to 50 nm (Figure 4H). To accelerate the growth of these spines, the films were immersed in a fresh solution of $(NH_4)_2TiF_6$ and H_3BO_3 for another 30 h. In this way, long nanorods ranging from 100 to 300 nm could be obtained (Figure 4I), which with their largely increased surface area should significantly improve the PEC cell performance. Moreover, the diameters of these nanorods are less than 10 nm, a feature that is beneficial to the surface photocatalysis for water splitting. As we know, for the small crystal grain sizes of the TiO_2 photoanode, the minority carrier diffusion length is limited to ~10 nm. In other words, only the photons absorbed within 10 nm of the TiO_2 surface[40,41] will contribute to the photocatalytic splitting of water. Therefore, our as-prepared photoelectrodes made of the branched TiO_2 NTs will be particularly expedient due to the ultrathin nanospines and the mechanically robust network. The high-resolution (HR) TEM image in Figure 4J and its corresponding SAED pattern reveal these spines are single-crystalline and grow along the [001] direction. EDS analysis shown in Supporting Information Figure S5D shows only the Ti and O peaks, in agreement with the high-resolution Ti and O XPS spectra, which are similar to those of the commercial P25 TiO_2 NPs (Supporting Information Figure S6).

To investigate the effectiveness of TiO_2 deposited on the 3D spiked substrates for PEC water splitting, we first coated standard Degussa P25 TiO_2 NPs on them by the doctor-blading method. The thickness was approximately 3 μm (see SEM images in Supporting Information Figure S7). Figure 5A shows a set of linear-sweep voltammagrams (reported with respect to the reversible hydrogen electrode (RHE), $E_{(RHE)} = E_{(Ag/AgCl)} + 0.1976\ V + 0.059\ pH$) recorded on three different thin films illuminated with chopped AM 1.5 light of 100 mW cm^{-2} intensity. Upon sweeping the potential from 0 to 1 V vs RHE under illumination, the P25 TiO_2 NPs deposited on both flat substrates (FTO-coated glass and FTO-coated flat Al@Al_2O_3@Ti/Pt) showed similar photoresponse with a photocurrent density of 0.08 mA cm^{-2} at 0.5 V vs RHE. Notably, the photocurrent density of the P25 NPs deposited on the spiked substrate showed ~2.3 times enhancement up to 0.18 mA cm^{-2} at the same applied potential. The significant enhancement of the photocurrent for P25 TiO_2 NPs deposited on the spiked substrate is believed to be the more rapid charge separation as compared to P25 TiO_2 NPs deposited on the flat substrate.

Semiconductor charge transport behaviors can be obtained from intensity modulated photocurrent spectroscopy (IMPS),[38,42] which is widely used in electron transport

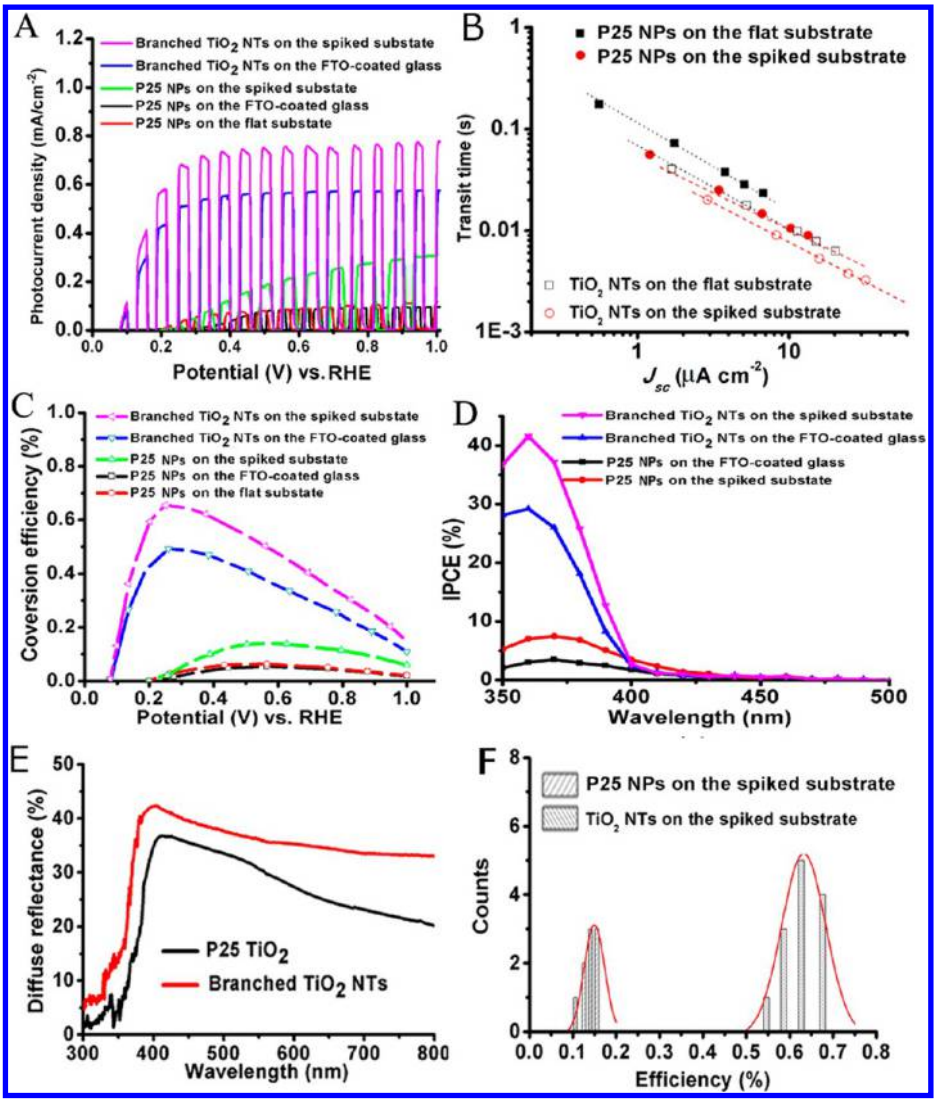

Figure 5. Photoelectrochemical performance of TiO_2 on the spiked substrates. (A) Chopped $J-V$ curves under xenon lamp illumination using a three-electrode setup (TiO_2 working, Pt counter, Ag/AgCl reference electrode, scan rate of 20 mV/s) show higher photoresponses for the two types of TiO_2 on the spiked substrate than on the flat substrate. (B) The average transit time of photogenerated electrons at 0.5 V vs RHE as a function of the maximal photocurrent density (J_{sc}) for P25 TiO_2 NPs deposited on the flat substrate and on the spiked substrate. A 368 nm LED lamp was used as the light source for the IMPS measurement. (C) Photoconversion efficiency of five different photoelectrodes as a function of applied potential based on the calculation reported previously.[5] (D) IPCEs for P25 TiO_2 NPs and branched TiO_2 NTs deposited on the flat substrate or on the spiked substrate, measured in the incident light wavelength range of 350−500 nm. Both P25 TiO_2 NPs samples on different substrates were measured at a potential of +0.55 V vs RHE, and both branched TiO_2 NTs on different substrates were measured at a potential of +0.25 V vs RHE. (E) Diffuse reflectance spectra of the branched TiO_2 NTs and commercial P25 TiO_2 NPs. (F) The efficiency distributions of the TiO_2 NTs and P25 NPs on the spiked substrate measured over 10 devices.

characterization of dye-sensitized solar cells. The average time of photogenerated electrons need to reach the photoelectrode, the transit time τ_d, can be estimated from $\tau_d = 1/2\pi f_{max}$, where "f_{max}" is the frequency at which the minimum in the IMPS plot occurs. Figure 5B plots τ_d of photogenerated electrons as a function of the maximal photocurrent density (J_{sc}) for P25 TiO_2 NPs and TiO_2 NTs deposited on the flat substrate and spiked substrate, respectively. Obviously, the electron transport for P25 TiO_2 NPs and TiO_2 NTs on the spiked substrate is faster than for their corresponding samples on the flat substrate, suggesting that the 3D spiked substrate can shorten electron transport length and therefore quicken charge separation. In addition, the transport time for TiO_2 NTs on the flat substrate is also shorter than that for P25 TiO_2 NPs on the same substrate. Therefore, the short electron transport length can improve charge-collection efficiency and thus enhance photoconversion efficiency.

The photoconversion efficiency for P25 TiO_2 NPs on the spiked substrate is twice greater than that on the flat substrate (Figure 5C). The result is in fairly good agreement with the IPCE measurements (Figure 5D), which revealed a peak of 7.4% at ~370 nm for P25 TiO_2 NPs on the spiked substrate but only 3.4% on the flat substrate. To take advantage of the spiked substrate for better charge-collection efficiency, the branched TiO_2 NTs were deposited on such substrate as a photoanode for PEC water splitting measurements. It should be noted that the film derived from the branched TiO_2 NTs shows a stronger light scattering capability in the near-infrared region than that from the standard Degussa P25 TiO_2 NPs (Figure 5E), which could also be beneficial to dye-sensitized solar cells.[43]

dx.doi.org/10.1021/jp507800t | J. Phys. Chem. C 2014, 118, 22465−22472

To understand the intrinsic carrier kinetic properties, we first conducted electrochemical impedance spectroscopic (EIS) measurements[44,45] on Degussa P25 TiO_2 NPs and the branched TiO_2 NTs on the FTO-coated glass in the electrolyte solution, at a frequency of 1 kHz in the dark coupled with Mott−Schottky (MS) analysis. The Mott−Schottky equation, which allows determination of charge carrier density (N_d) and flat-band potential (V_{FB}), can be expressed as

$$\frac{1}{C^2} = \frac{2}{e_0 \varepsilon \varepsilon_0 N_D}\left[(V - V_{FB}) - \frac{kT}{e_0}\right]$$

where e_0 is the electron charge, ε is the dielectric constant of TiO_2, ε_0 is the permittivity of vacuum, N_d is the dopant density, V is the potential difference across the semiconductor space-charge region, V_{FB} is the flatband potential, and kT/e_0 is a temperature-dependent correction term. It shows that when $1/C^2$ is zero, the x-intercept is equal to the flat band potential V_{FB}, and the dopant density N_D can be determined from the slope of the linear region:

$$N_D = \frac{2}{e_0 \varepsilon \varepsilon_0}\left[\frac{d\left(\frac{1}{C^2}\right)}{dV}\right]^{-1}$$

As shown in Supporting Information Figure S8B, the flat band potential V_{FB} can be estimated to be 0.14 V vs RHE for the P25 TiO_2 nanoparticles, but a negative shift from 0.14 to 0.03 V vs Ag/AgCl was observed for the branched TiO_2 NTs. The reason probably was the existence of high level surface states in P25 TiO_2 NPs, which can act as charge carrier recombination centers or trapping states. Additionally, both samples show a positive slope in the Mott−Schottky plots ($1/C^2$ versus V), indicating the n-type nature of the P25 TiO_2 NPs and branched TiO_2 NTs. However, the branched TiO_2 NTs show a much lower slope of the linear regions as compared to the P25 TiO_2 NPs, clearly suggesting a much higher value of the dopant density in the branched TiO_2 NTs. Using $\varepsilon = 48$[46] for calculation, the electron densities of the P25 TiO_2 NPs and branched TiO_2 NTs were 3.4×10^{17} and 9.8×10^{17} cm^{-3}, respectively. The enhanced donor density means the increased electron density for n-type TiO_2,[47] which could lead to improved charge transport, as well as the electron transfer at the interface between the semiconductor and the FTO substrate.

The PEC measurement (Figure 5A) revealed for the P25 TiO_2 photoelectrode an onset of the photocurrent at 0.18 V vs RHE, which rose to 0.08 mA cm^{-2} at 0.5 V vs RHE. For the film made of the branched TiO_2 NTs, we observed a significant photoresponse enhancement, which started at 0.08 V and reached a photocurrent density of 0.54 mA cm^{-2} at 0.35 V vs RHE. This is in accordance with a ∼100 mV negative shift of flat band potential for the branched TiO_2 NTs. The significant photocurrent enhancement can be ascribed to an improved charge separation due to the increased donor densities of the branched TiO_2 NTs capped with ultrathin nanowires, as well as the highly efficient electronic transport of the 3D NT network. Significantly, the branched TiO_2 NTs on the spiked substrate showed a large enhancement in photoresponse with a photocurrent density of 0.73 mA cm^{-2} at the same applied voltage, which is ∼1.3 times higher than that of the branched TiO_2 NTs on the flat substrate. Additionally, the statistical histograms in Figure 5F indicated that the photoelectrode conversion efficiency of the TiO_2 NTs on the spiked substrate is much higher than that of P25 NPs on the same substrate. Notably, our branched TiO_2 NTs can reach a photocurrent onset and a saturation photocurrent at a lower potential than the P25 TiO_2 NPs, indicating that only a lower applied bias is required to achieve the maximum of the overall conversion efficiency. As shown in Figure 5C, with the P25 TiO_2 NPs on the spiked substrate, the maximum photoelectrode efficiency of ∼0.15% was achieved at applied voltage of +0.55 V vs RHE, which is much higher than that on the flat substrate (only ∼0.06%) at the same applied voltage. More impressively, for the branched TiO_2 NTs, we obtained a maximum efficiency of 0.66% and 0.55% on the spiked substrate and on the flat substrate, respectively, at applied voltage of +0.25 V vs RHE. The applied potential obtained from the branched TiO_2 NTs with the same efficiency is lower than the recently reported values with pure TiO_2 nanowires and nanotubes.[18,21] In other words, the peculiar architecture can achieve good performance at a low potential. The results thus validate the unique benefit of our branched TiO_2 NTs and the 3D spiked substrate to the PEC performance.

To further understand the enhanced overall PEC conversion of the branched TiO_2 NTs on the spiked substrates, we also performed incident-photon-to-current-conversion efficiency (IPCE) measurements as a function of incident light wavelength (Figure 5D). IPCE is expressed as IPCE = $(1240 \times I)/(\lambda \times P_{light})$, where I is the photocurrent density (mA cm^{-2}), λ is the incident light wavelength (nm), and P_{light} (mW cm^{-2}) is the power density of monochromatic light at a specific wavelength. The overwhelming observation is that, in comparison to the flat substrate, covered with the branched TiO_2 NTs, the spiked substrate exhibited much enhanced PEC activity across the entire UV spectral region. Such enhancement is presumably due to the improved charge separation arising from the short electron transport distance purposely built into the 3D nanospike array.

4. CONCLUSIONS

We have successfully prepared the branched TiO_2 by dissolution and nucleation processes with the assistance of ZnO nanotetrapods template. The branched TiO_2 NTs on the flat substrate as a photoelectrode for PEC water splitting could yield an improved photocurrent density of 0.54 mA cm^{-2} at 0.35 V vs RHE as compared to that of P25 TiO_2 NPs at 0.55 V vs RHE. Significantly, when they were deposited on the 3D spiked substrates, the photocurrent density has surged to 0.73 mA cm^{-2} at the same applied voltage. This resultant photoelectrode efficiency was significantly higher than those for the branched TiO_2 nanowire and nanotube photoelectrode at a low applied bias due to the unique architecture of tetrapods-based network consisting of ultrathin TiO_2 nanowires and the 3D spiked substrate. As a whole, our work has opened a promising avenue to developing high-efficiency PEC photoelectrodes on the 3D substrates for photoelectrochemical water splitting.

■ ASSOCIATED CONTENT

Supporting Information

Other characterizations including SEM image of the surface of an Al piece, optical microscopy and light-scattering spectroscopy of the flat Al and the spiked Al substrates, schematic drawing illustrating the growth of the branched TiO_2 NTs, XRD patterns, EDS analysis and XPS spectrum, SEM images of

dx.doi.org/10.1021/jp507800t | J. Phys. Chem. C 2014, 118, 22465−22472

P25 TiO_2 NPs deposited on the spiked substrate, and electrochemical impedance spectra of the branched TiO_2 NTs and commercial P25 TiO_2 NPs. This material is available free of charge via the Internet at http://pubs.acs.org.

AUTHOR INFORMATION

Corresponding Authors

*Phone: +852 2358-8027. E-mail: eezfan@ust.hk.
*Phone: +852 2358-7362. E-mail: chsyang@ust.hk.

Author Contributions

[‖]These authors contributed equally.

Notes

The authors declare no competing financial interest.

ACKNOWLEDGMENTS

This work was supported by the HK-RGC General Research Funds (GRF nos. HKUST 605710, 604809, 612111, 612113), partially supported by ITS/117/13 from Hong Kong Innovation Technology Commission, HKUST Research Project Competition Grant (RPC11EG38), the National Natural Science Foundation of China (21403287 and 21433013), the National Science Foundation for Postdoctoral Scientists of China (014M550314), and the Natural Science Foundation of Jiangsu Province, China (BK20140383).

REFERENCES

(1) Fujishima, A. Electrochemical Photolysis of Water at a Semiconductor Electrode. *Nature* **1972**, *238*, 37−38.

(2) Chen, X.; Shen, S.; Guo, L.; Mao, S. S. Semiconductor-based Photocatalytic Hydrogen Generation. *Chem. Rev.* **2010**, *110*, 6503−6570.

(3) Zou, Z.; Ye, J.; Sayama, K.; Arakawa, H. Direct Splitting of Water under Visible Light Irradiation with an Oxide Semiconductor Photocatalyst. *Nature* **2001**, *414*, 625−627.

(4) Lewis, N. S.; Nocera, D. G. Powering the Planet: Chemical Challenges in Solar Energy Utilization. *Proc. Natl. Acad. Sci. U.S.A.* **2006**, *103*, 15729−15735.

(5) Walter, M. G.; Warren, E. L.; McKone, J. R.; Boettcher, S. W.; Mi, Q.; Santori, E. A.; Lewis, N. S. Solar Water Splitting Cells. *Chem. Rev.* **2010**, *110*, 6446−6473.

(6) Zhang, W.; Yang, S. In Situ Fabrication of Inorganic Nanowire Arrays Grown from and Aligned on Metal Substrates. *Acc. Chem. Res.* **2009**, *42*, 1617−1627.

(7) Tilley, S. D.; Cornuz, M.; Sivula, K.; Grätzel, M. Light-Induced Water Splitting with Hematite: Improved Nanostructure and Iridium Oxide Catalysis. *Angew. Chem., Int. Ed.* **2010**, *49*, 6504−6508.

(8) Cho, I. S.; Chen, Z.; Forman, A. J.; Kim, D. R.; Rao, P. M.; Jaramillo, T. F.; Zheng, X. Branched TiO_2 Nanorods for Photoelectrochemical Hydrogen Production. *Nano Lett.* **2011**, *11*, 4978−4984.

(9) Su, J.; Guo, L.; Bao, N.; Grimes, C. A. Nanostructured WO_3/$BiVO_4$ Heterojunction Films for Efficient Photoelectrochemical Water Splitting. *Nano Lett.* **2011**, *11*, 1928−1933.

(10) Chen, W.; Zhang, H.; Hsing, I. M.; Yang, S. A New Photoanode Architecture of Dye Sensitized Solar Cell Based On ZnO Nanotetrapods with No Need for Calcination. *Electrochem. Commun.* **2009**, *5*, 1057−1060.

(11) Qiu, Y.; Leung, S.; Zhang, Q.; Hua, B.; Lin, Q.; Wei, Z.; Tsui, K.; Zhang, Y.; Yang, S.; Fan, Z. Efficient Photoelectrochemical Water Splitting with Ultrathin films of Hematite on Three-Dimensional Nanophotonic Structures. *Nano Lett.* **2014**, *14*, 2123−2129.

(12) Joya, K. S.; Joya, Y. F.; Ocakoglu, K.; van de Krol, R. Water-Splitting Catalysis and Solar Fuel Devices: Artificial Leaves on the Move. *Angew. Chem., Int. Ed.* **2013**, *52*, 10426−10437.

(13) Lee, M. H.; Takei, K.; Zhang, J.; Kapadia, R.; Zheng, M.; Chen, Y.; Nah, J.; Matthews, T. S.; Chueh, Y.; Ager, J. W. p-Type InP Nanopillar Photocathodes for Efficient Solar-Driven Hydrogen Production. *Angew. Chem., Int. Ed.* **2012**, *51*, 10918−10922.

(14) Ling, Y.; Wang, G.; Wheeler, D. A.; Zhang, J. Z.; Li, Y. Sn-Doped Hematite Nanostructures for Photoelectrochemical Water Splitting. *Nano Lett.* **2011**, *11*, 2119−2125.

(15) Su, J.; Feng, X.; Sloppy, J. D.; Guo, L.; Grimes, C. A. Vertically Aligned WO_3 Nanowire Arrays Grown Directly on Transparent Conducting Oxide Coated Glass: Synthesis and Photoelectrochemical Properties. *Nano Lett.* **2010**, *10*, 203−208.

(16) Feng, X.; Shankar, K.; Varghese, O. K.; Paulose, M.; Latempa, T. J.; Grimes, C. A. Vertically Aligned Single Crystal TiO_2 Nanowire Arrays Grown Directly on Transparent Conducting Oxide Coated Glass: Synthesis Details and Applications. *Nano Lett.* **2008**, *8*, 3781−3786.

(17) Shankar, K.; Basham, J. I.; Allam, N. K.; Varghese, O. K.; Mor, G. K.; Feng, X.; Paulose, M.; Seabold, J. A.; Choi, K.; Grimes, C. A. Recent Advances in the Use of TiO_2 Nanotube and Nanowire Arrays for Oxidative Photoelectrochemistry. *J. Phys. Chem. C* **2009**, *113*, 6327−6359.

(18) Mor, G. K.; Shankar, K.; Paulose, M.; Varghese, O. K.; Grimes, C. A. Enhanced Photocleavage of Water Using Titania Nanotube Arrays. *Nano Lett.* **2005**, *5*, 191−195.

(19) Wang, G.; Ling, Y.; Wheeler, D. A.; George, K. E. N.; Horsley, K.; Heske, C.; Zhang, J. Z.; Li, Y. Facile Synthesis of Highly Photoactive alpha-Fe_2O_3-Based Films for Water Oxidation. *Nano Lett.* **2011**, *11*, 3503−3509.

(20) Wang, G.; Wang, H.; Ling, Y.; Tang, Y.; Yang, X.; Fitzmorris, R. C.; Wang, C.; Zhang, J. Z.; Li, Y. Hydrogen-Treated TiO_2 Nanowire Arrays for Photoelectrochemical Water Splitting. *Nano Lett.* **2011**, *11*, 3026−3033.

(21) Xu, M.; Da, P.; Wu, H.; Zhao, D.; Zheng, G. Controlled Sn-Doping in TiO_2 Nanowire Photoanodes with Enhanced Photoelectrochemical Conversion. *Nano Lett.* **2012**, *12*, 1503−1508.

(22) Du, C.; Yang, X.; Mayer, M. T.; Hoyt, H.; Xie, J.; McMahon, G.; Bischoping, G.; Wang, D. Hematite-Based Water Splitting with Low Turn-On Voltages. *Angew. Chem., Int. Ed.* **2013**, *52*, 12692−12695.

(23) Sartori1, A.; Visentin, F.; El Habra, N.; De Zorzi1, C.; Natali, M.; Garoli, D.; Gerbasi, R.; Casarin, M.; Rossetto, G. Preparation of Tetrapod-like ZnO/TiO_2 Core-Shell Nanostructures as Photocatalytic Powder. *Crys. Res. Technol.* **2011**, *46*, 885−890.

(24) Wang, G.; Ling, Y.; Wang, H.; Lu, X. Chemically Modified Nanostructures for Photoelectrochemical Water Splitting. *J. Photochem. Photobiol., C* **2014**, *19*, 35−51.

(25) Pesci, F. M.; Wang, G.; Klug, D. R.; Li, Y.; Cowan, A. J. Efficient Suppression of Electron−Hole Recombination in Oxygen-Deficient Hydrogen-Treated TiO_2 Nanowires for Photoelectrochemical Water Splitting. *J. Phys. Chem. C* **2013**, *117*, 25837−25844.

(26) Zhou, M.; Wu, H. B.; Bao, J.; Liang, L.; Lou, X. W. D.; Xie, Y. Ordered Macroporous $BiVO_4$ Architectures with Controllable Dual Porosity for Efficient Solar Water Splitting. *Angew. Chem., Int. Ed.* **2013**, *52*, 8579−8583.

(27) Hou, Y.; Zuo, F.; Dagg, A.; Feng, P. A Three-Dimensional Branched Cobalt-doped α-Fe_2O_3 Nanorod/$MgFe_2O_4$ Heterojunction Array as a Flexible Photoanode for Efficient Photoelectrochemical Water Oxidation. *Angew. Chem., Int. Ed.* **2013**, *52*, 1248−1252.

(28) Tétreault, N.; Arsenault, É.; Heiniger, L.; Soheilnia, N.; Brillet, J.; Moehl, T.; Zakeeruddin, S.; Ozin, G. A.; Grätzel, M. High-Efficiency Dye-Sensitized Solar Cell with Three-Dimensional Photoanode. *Nano Lett.* **2011**, *11*, 4579−4584.

(29) Stefik, M.; Cornuz, M.; Mathews, N.; Hisatomi, T.; Mhaisalkar, S.; Graetzel, M. Transparent, Conducting Nb:SnO_2 for Host-Guest Photoelectrochemistry. *Nano Lett.* **2012**, *12*, 5431−5435.

(30) Leung, S.; Gu, L.; Zhang, Q.; Tsui, K.; Shieh, J.; Shen, C.; Hsiao, T.; Hsu, C.; Lu, L.; Li, D.; et al. Roll-to-Roll Fabrication of Large Scale and Regular Arrays of Three-Dimensional Nanospikes for High Efficiency and Flexible Photovoltaics. *Sci. Rep.* **2014**, 4243.

(31) Leung, S. F.; Yu, M.; Lin, Q.; Kwon, K.; Ching, K. L.; Gu, L.; Yu, K.; Fan, Z. Efficient Photon Capturing with Ordered Three-Dimensional Nanowell Arrays. *Nano Lett.* **2012**, *12*, 3682−3689.

(32) Leung, S.; Zhang, Q.; Xiu, F.; Yu, D.; Ho, J. C.; Li, D.; Fan, Z. Light Management with Nanostructures for Optoelectronic Devices. *J. Phys. Chem. Lett.* **2014**, *5*, 1479−1495.
(33) Lin, Q.; Leung, S.; Lu, L.; Chen, X.; Chen, Z.; Tang, H.; Su, W.; Li, D.; Fan, Z. Efficient Light Absorption with Integrated Nanopillar/Nanowell Arrays for Three-Dimensional Thin-Film Photovoltaic Applications. *ACS Nano* **2014**, *7*, 2725−2732.
(34) Qiu, Y.; Yan, K.; Deng, H.; Yang, S. Secondary Branching and Nitrogen Doping of ZnO Nanotetrapods: Building a Highly Active Network for Photoelectrochemical Water Splitting. *Nano Lett.* **2012**, *1*, 407−413.
(35) Chen, W.; Qiu, Y.; Zhong, Y.; Wong, K. S.; Yang, S. High-Efficiency Dye-Sensitized Solar Cells Based on the Composite Photoanocles of SnO2 Nanoparticles/ZnO Nanotetrapods. *J. Phys. Chem. A* **2010**, *114*, 3127−3138.
(36) Yu, R.; Ching, K.; Lin, Q.; Leung, S.; Arcrossito, D.; Fan, Z. Strong Light Absorption of Self-Organized 3-D Nanospike Arrays for Photovoltaic Applications. *ACS Nano* **2011**, *5*, 9291−9298.
(37) Qiu, Y.; Yang, S. ZnO Nanotetrapods: Controlled Vapor-Phase Synthesis and Application for Humidity Sensing. *Adv. Funct. Mater.* **2007**, *17*, 1345−1352.
(38) Qiu, Y.; Chen, W.; Yang, S. Double-Layered Photoanodes from Variable-Size Anatase TiO2 Nanospindles: A Candidate for High-Efficiency Dye-Sensitized Solar Cells. *Angew. Chem., Int. Ed.* **2010**, *49*, 3675−3679.
(39) Xu, C.; Shin, P. H.; Cao, L.; Wu, J.; Gao, D. Ordered TiO_2 Nanotube Arrays on Transparent Conductive Oxide for Dye-Sensitized Solar Cells. *Chem. Mater.* **2009**, *22*, 143−148.
(40) Leng, W.; Barnes, P. R.; Juozapavicius, M.; O'Regan, B. C.; Durrant, J. R. Electron Diffusion Length in Mesoporous Nanocrystalline TiO_2 Photoelectrodes during Water Oxidation. *J. Phys. Chem. Lett.* **2010**, *6*, 967−972.
(41) Arango, A. C.; Johnson, L. R.; Bliznyuk, V. N.; Schlesinger, Z.; Carter, S. A.; Hörhold, H. Efficient Titanium Oxide/Conjugated Polymer Photovoltaics for Solar Energy Conversion. *Adv. Mater.* **2000**, *12*, 1689−1692.
(42) Zhu, K.; Neale, N. R.; Miedaner, A.; Frank, A. J. Enhanced Charge-Collection Efficiencies and Light Scattering in Dye-Sensitized Solar Cells Using Oriented TiO_2 Nanotubes Arrays. *Nano Lett.* **2007**, *7*, 69−74.
(43) Zhang, Q.; Dandeneau, C. S.; Zhou, X.; Cao, G. ZnO Nanostructures for Dye-Sensitized Solar Cells. *Adv. Mater.* **2009**, *21*, 4087−4108.
(44) Tse, K.; Nichols, B. M.; Yang, W.; Butler, J. E.; Russell, J. N.; Hamers, R. J. Electrical Properties of Diamond Surfaces Functionalized with Molecular Monolayers. *J. Phys. Chem. B* **2005**, *109*, 8523−8532.
(45) Perkins, C. L.; Lee, S.; Li, X.; Asher, S. E.; Coutts, T. J. Identification of Nitrogen Chemical States in N-doped ZnO via X-Ray Photoelectron Spectroscopy. *J. Appl. Phys.* **2005**, *97*, 034907.
(46) Wang, G.; Wang, Q.; Lu, W.; Li, J. Photoelectrochemical Study on Charge Transfer Properties of TiO_2-B Nanowires with an Application as Humidity Sensors. *J. Phys. Chem. B* **2006**, *110*, 22029−22034.
(47) Janotti, A.; Varley, J.; Rinke, P.; Umezawa, N.; Kresse, G.; Van de Walle, C. Hybrid Functional Studies of the Oxygen Vacancy in TiO_2. *Phys. Rev. B* **2010**, *81*, 085212.